High-Pressure Structural Transitions of Sc2O3 by X-ray Diffraction, Raman Spectra, and Ab Initio Calculations

11 AUTHORS, INCLUDING:

Yinwei Li
Jiangsu Normal University
49 PUBLICATIONS **451** CITATIONS

Jian Hao
Jiangsu Normal University
33 PUBLICATIONS **214** CITATIONS

Qiliang Cui
Jilin University
115 PUBLICATIONS **1,175** CITATIONS

Inorganic Chemistry

High-Pressure Structural Transitions of Sc_2O_3 by X-ray Diffraction, Raman Spectra, and Ab Initio Calculations

Dan Liu, Weiwei Lei, Yinwei Li, Yanming Ma, Jian Hao, Xiaohui Chen, Yunxia Jin, Dedi Liu, Shidan Yu, Qiliang Cui,* and Guangtian Zou

State Key Laboratory of Superhard Materials, Jilin University, Changchun 130012, People's Republic of China

The high-pressure behavior of scandium oxide (Sc_2O_3) has been investigated by angle-dispersive synchrotron powder X-ray diffraction and Raman spectroscopy techniques in a diamond anvil cell up to 46.2 and 42 GPa, respectively. An irreversible structural transformation of Sc_2O_3 from the cubic phase to a monoclinic high-pressure phase was observed at 36 GPa. Subsequent ab initio calculations for Sc_2O_3 predicted the phase transition from the cubic to monoclinic phase but at a much lower pressure. The same calculations predicted a second phase transition at 77 GPa from the monoclinic to hexagonal phase.

1. Introduction

The rare-earth sesquioxides have recently attracted particular attention because of their unique physical and chemical properties and potential applications in nuclear engineering,[1-3] light-triggered semiconductor devices,[4] and antireflection coatings.[5] Scandium oxide, Sc_2O_3, is sometimes considered as a rare-earth sesquioxide because of its similar chemical behavior.[6] It has many applications in various fields of technologies. It can be used as laser optical coatings because of its high refractive index and high damage threshold.[7-10] It is also a good candidate for applications in photonics and optoelectronics because of its chemical stabi-

lity and high ultraviolet cutoff.[11,12] In recent years, there have been many studies on the polymorphs of rare-earth sesquioxides.[13-17] So far, five structural modifications have been identified in the rare-earth sesquioxides.[18-20] Three phases, designated as A (hexagonal, space group $P\bar{3}m1$) with each cation surrounded by seven anions, B (monoclinic, space group $C2/m$) with six- or seven-coordinated cation sites, and C (cubic, space group $Ia\bar{3}$) with six-coordinated cations, are commonly observed at ambient temperature and pressure. The other two phases denoted as H (hexagonal, space group $P6_3/mmc$) and X (cubic, space group $Im\bar{3}m$) are formed at very high temperatures.[21]

At ambient conditions, the molar volume of rare-earth sesquioxides decreases in the sequence of C → B → A with increasing cation coordination number. Hence, high pressure is expected to produce similar sequential changes.[22] At ambient conditions, the thermodynamically stable phase of Sc_2O_3 has a C-type structure. It has been reported that Sc_2O_3 remains in a cubic phase up to the melting point without

*To whom correspondence should be addressed. E-mail: cql@jlu.edu.cn.

(1) Shikama, T.; Yasuda, K.; Yamamoto, S.; Tsuchiya, B.; Yamauchi, M.; Nishitani, T.; Suzuki, T.; Okamoto, K.; Kubo, N. *Nucl. Fusion* **2006**, *46*, 46.

(2) Weber, W. J.; Ewing, R. C.; Catlow, C. R.; de la Rubia, T. D.; Hobbs, L. W.; Kinoshitam, C.; Matzkem, H.; Motta, A. T.; Nastasi, M.; Salje, E. H.; Vance, E. R.; Zinkle, S. J. *J. Mater. Res.* **1998**, *13*, 1434.

(3) Kinoshita, C.; Zinkle, S. J. *J. Nucl. Mater.* **1996**, *100*, 233.

(4) Qadri, S. B.; Kim, H.; Yousuf, M.; Khan, H. R. *Appl. Surf. Sci.* **2003**, *208–209*, 611.

(5) Heitmann, W. *Appl. Opt.* **1973**, *12*, 394.

(6) Ubaldini, A.; Carnasciali, M. M. *J. Alloys Compd.* **2008**, *454*, 374.

(7) Grosso, D.; Sermon, P. A. *Thin Solid Films* **2000**, *368*, 116.

(8) Xu, Z.; Daga, A.; Chen, H. *Appl. Phys. Lett.* **2001**, *79*, 3728.

(9) Rainer, F.; Lowdermilk, W. H.; Milam, D.; Hart, T.; Lichtenstein, T. L.; Carniglia, C. K. *Appl. Opt.* **1982**, *21*, 3685.

(10) Tamura, S.; Kimura, S.; Sato, Y.; Yoshida, H.; Yoshida, K. *Jpn. J. Appl. Phys.* **1992**, *31*, 2762.

(11) Horowitz, C. T.; Gschneidner, G. A. *Scandium*; Academic: New York, 1975.

(12) Krsmanović, R.; Lebedev, O. I.; Speghini, A.; Bettinelli, M.; Polizzi, S.; Van Tendeloo, G. *Nanotechnology* **2006**, *17*, 2805.

(13) Meyer, C.; Sanchez, J. P.; Thomasson, J. *Phys. Rev. B* **1995**, *51*, 12187.

(14) Dilawar, N.; Varandani, D.; Mehrotra, S.; Poswal, H. K.; Sharma, S. M.; Bandyopadhyay, A. K. *Nanotechnology* **2008**, *19*, 115703.

(15) Guo, Q. X.; Zhao, Y. S.; Jiang, C.; Mao, W. L.; Wang, Z. W. *Solid State Commun.* **2008**, *145*, 250.

(16) Dilawar, N.; Varandani, D.; Pandey, V. P.; Kumar, M.; Shivaprasad, S. M.; Sharma, P. K.; Bandyopadhyay, A. K. V. *J. Nanosci. Nanotechnol.* **2006**, *6*, 105.

(17) Zhang, F. X.; Lang, M.; Wang, J. W.; Becker, U.; Ewing, R. C. *Phys. Rev. B* **2008**, *78*, 064114.

(18) Chikalla, T. D.; McNeilly, E.; Roberts, J. *J. Am. Ceram. Soc.* **1972**, *55*, 428.

(19) Haire, R. G.; Eyring, L. Comparisons of the binary oxides. In *Handbook on the physics and chemistry of the rare earths. Lanthanides/actinides: chemistry*; Gschneidner, K. A., Jr., Eyring, L., Choppin, G. R., Lander, G. R., Eds.; Elsevier Science: Amsterdam, The Netherlands, 1994; Vol. *18*, p 413.

(20) Tang, M.; Lu, P.; Valdez, J. A.; Sickafus, K. E. *J. Appl. Phys.* **2006**, *99*, 063514.

(21) Foex, M.; Traverse, J. P. *Rev. Int. High Temp. Refract.* **1966**, *3*, 429.

(22) Zinkevich, M. *Prog. Mater. Sci.* **2007**, *52*, 597.

phase transition at room pressure.[23] Reid and Ringwood reported that the C-type Sc_2O_3 transformed to the B type at 10−15 GPa and 1000 °C.[24] Atou et al. demonstrated that the C → B transition of Sc_2O_3 did not occur by shock compressions at 20 and 40 GPa.[25] They found that the X-ray diffraction (XRD) lines slightly broadened compared with those of the initial C type. Later, they estimated that the C → A transition occurred at 40.9 GPa from analysis of the shock compression curve.[26] However, high-pressure data obtained under shock conditions cannot provide continuous tuning of the pressure. Thus, it needs to employ new probing techniques that allow in situ measurements. Wu et al. predicted the B → A phase transition of Sc_2O_3 at around 75 GPa based on theoretical calculations.[27] Zinkevich pointed out that the volume change of such a transition exceeds the corresponding values of other rare-earth sesquioxides.[22] However, up to now, there has not been enough experimental evidence to confirm that Sc_2O_3 transforms from the C type to the B type or directly to the A type. Recently, Yusa et al.[28] observed that B-type Sc_2O_3 undergoes a phase transition to the Gd_2S_3 structure at high temperatures and high pressures; however, no phase transformation was found up to 31 GPa at room temperature.

In order to understand the structural behavior of Sc_2O_3 under high pressures and to verify the theoretical prediction and shock-induced high-pressure data, we have carried out a comprehensive investigation of Sc_2O_3 at room temperature by synchrotron-radiation XRD and Raman spectra using a diamond anvil cell (DAC) up to 46.2 and 42 GPa, respectively. We found a pressure-induced irreversible phase transition at 36 GPa. On the basis of the structural refinement of XRD data, we provide a detailed structural and lattice dynamical description of this high-pressure phase. The phase stabilities and phase transitions between C, B, and A are discussed in the context of ab initio calculations of the enthalpies for the three phases.

2. Experimental Procedures

Commercially available Sc_2O_3 powder (99.99%) was loaded into a gasketed high-pressure DAC with a culet face of 400 μm diameter. The structure of the sample was confirmed to be the cubic form, corresponding to C-Sc_2O_3. The sample powder and ruby particles were loaded into the high-pressure chamber, and a small hole (120 μm diameter and 50 μm thickness) was drilled at the center of a preindented stainless steel gasket and filled with a mixture of 16:3:1 of methanol/ethanol/water as the pressure-transmitting medium. The pressure was determined from the frequency shift of the ruby R1 fluorescence line.[29] The measured pressure difference of various ruby chips was less than 2 GPa. The R1 and R2 lines of the ruby fluorescence signal remained well separated throughout the experiments, indicating that a good quasi-hydrostatic condition was maintained even when the pressure medium was solidified. In situ high-pressure

angle-dispersive XRD experiments were carried out up to 46.2 GPa using synchrotron X-ray of the X17B3 station of the National Synchrotron Light Source, Brookhaven National Laboratory, Upton, NY. A monochromatic beam with a wavelength of 0.385 621 Å was used. The beam was focused to a spot of about 25 μm in size. The diffraction data were collected using a MAR165 CCD detector. The Bragg diffraction rings were recorded with an imaging plate detector, and the two-dimensional XRD images were analyzed using *FIT2D* software, yielding one-dimensional intensity versus diffraction angle 2θ patterns.[30] The average acquisition time was 200 s. The sample−detector distance and geometric parameters were calibrated using a CeO_2 standard from the National Institute of Standards and Technology (Gaithersburg, MD). Simulation and analysis of the XRD patterns at different pressures were performed using the Material Studio program. Unit-cell parameters were obtained using DICVOL91, and structure refinement (space group) was carried out using the Rietveld method.[31,32] During each refinement cycle, the scale factor, background parameter, and cell parameter were optimized.

High-pressure Raman spectra were recorded on a Renishaw inVia Raman microscope in backscattering geometry using the 514.5 nm line of an argon ion laser, provided with a CCD detector system. Pressure-induced shifts of overlapping Raman bands were analyzed by fitting the spectra to Lorentzian functions to determine the line-shape parameters. Experimental details regarding the Raman and ruby fluorescence systems are presented in the following sections.

3. Computational Procedures

The geometric optimization, phase-transition pressures, and enthalpy changes for the C, B, and A phases of Sc_2O_3 calculations were performed within the density functional theory (DFT) framework using a pseudopotential plane-wave method. We employed the all-electron projector augmented wave approach[33] within the Perdew−Burke−Ernzerhof parametrization of a generalized gradient approximation (GGA), as implemented in the Vienna ab initio simulation package code.[34] The plane-wave kinetic energy cutoff was set at 520 eV. The k-point meshes for the Brillouin zone sampling were constructed using the Monkhorst−Pack scheme.[35] We used $4 \times 4 \times 4$, $8 \times 8 \times 3$, and $10 \times 10 \times 6$ k-point meshes for the cubic (80-atom), monoclinic (30-atom), and hexagonal (5-atom) unit cells of Sc_2O_3, respectively. Such parameters were found to be sufficient to give fully converged results. For computational convenience, we performed energy calculations at $T = 0$ K, and thus the free energy reduces to enthalpy.

4. Results and Discussion

The schematic crystal structure of C-Sc_2O_3 is shown in Figure 1a. We can see two different types of Sc^{3+}, which occupy both octahedral and trigonal-prismatic interstices within the lattice of O^{2-} ions. The two different Sc and O atoms take up 8b, 24d, and 48e Wyckoff positions

(23) Weigel, F.; Scherer, V. *Radiochim. Acta* **1965**, *4*, 197.
(24) Reid, A. F.; Ringwood, A. E. *J. Geophys. Res.* **1969**, *74*, 3238.
(25) Atou, T.; Kusaba, K.; Fukuoka, K.; Kikuchi, M.; Syono, Y. *J. Solid State Chem.* **1990**, *89*, 378.
(26) Atou, T.; Kikuchi, M.; Fukuoka, K.; Syono, Y. *AIP Conf. Proc.* **1994**, *309*, 331.
(27) Wu, B.; Zinkevich, M.; Aldinger, F.; Wen, D. Z.; Chen, L. *J. Solid State Chem.* **2007**, *180*, 3280.
(28) Yusa, H.; Tsuchiya, T.; Sata, N.; Ohishi, Y. *Inorg. Chem.* **2009**, *48*, 7537–7543.
(29) Mao, H. K.; Xu, J.; Bell, P. M. *J. Geophys. Res.* **1986**, *91*, 4673.

(30) Hammersley, A. P.; Svensson, S. O.; Hanfland, M.; Fitch, A. N.; Hausermann, D. *High Press. Res.* **1996**, *14*, 235.
(31) Liu, D.; Lei, W. W.; Zou, B.; Yu, S. D.; Hao, J.; Wang, K.; Liu, B. B.; Cui, Q. L.; Zou, G. T. *J. Appl. Phys.* **2008**, *104*, 083506.
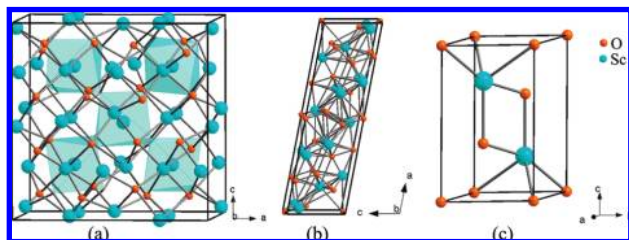(32) Liu, D.; Lei, W. W.; Hao, J.; Liu, D. D.; Liu, B. B.; Wang, X.; Chen, X. H.; Cui, Q. L.; Zou, G. T.; Liu, J.; Jiang, S. *J. Appl. Phys.* **2009**, *105*, 023513.
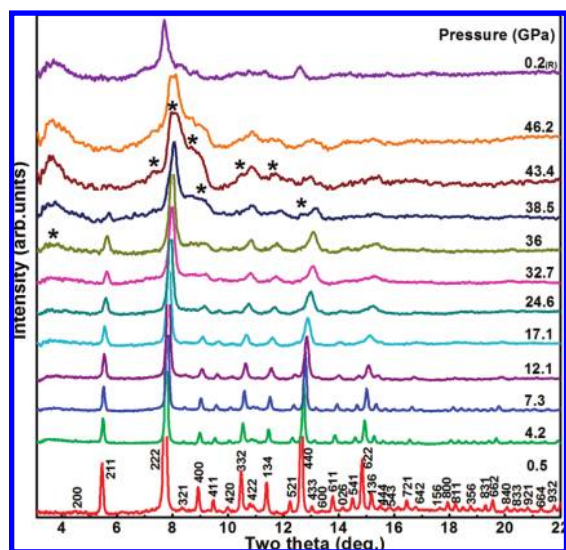(33) Blöchl, P. E. *Phys. Rev. B* **1994**, *50*, 17953.
(34) Kresse, G.; Joubert, D. *Phys. Rev. B* **1999**, *59*, 1758.
(35) Monkhorst, H. J.; Pack, J. D. *Phys. Rev. B* **1976**, *13*, 5188.
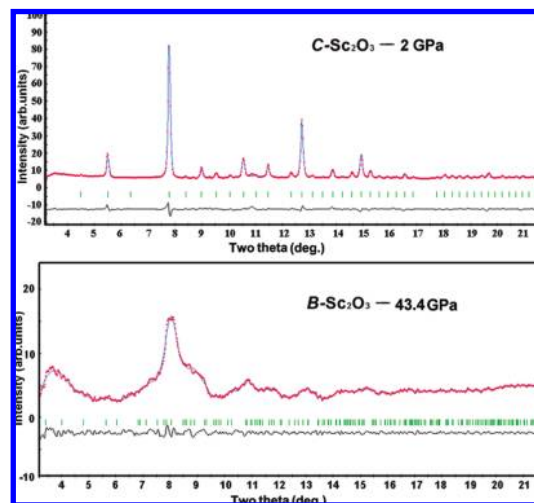
Figure 1. Crystal structures of (a) cubic C-Sc_2O_3, (b) monoclinic B-Sc_2O_3, and (c) hexagonal A-Sc_2O_3. Blue spheres represent the Sc atoms and yellow spheres the O atoms.

Figure 2. XRD patterns collected at various pressures for Sc_2O_3 with incident wavelength $\lambda = 0.385\,621$ Å. Asterisks show the appearance of new Bragg peaks corresponding to a monoclinic B type. The top panel is the XRD spectrum at 0.2 GPa after decompressing from 46.2 GPa.

Figure 3. Rietveld full-profile refinements of the diffraction patterns collected on compression at (a) 2 GPa and (b) at 43.4 GPa. In the C phase, the fit is good for the diffraction pattern shown, with $Rwp = 1.8\%$. The high-pressure B-phase fit is good for the diffraction pattern shown, with $Rwp = 4.0\%$. Red, blue, and black solid lines represent experimental, calculated, and residual patterns, respectively.

Table 1. Cell Parameters and Refined Fractional Coordinates for the $C2/m$ Phase of Sc_2O_3 at 38.5 GPa

| lattice parameters	a (Å)	b (Å)	c (Å)	β (deg)
(38.5 GPa)	13.142(2)	3.221(4)	7.773(4)	100.55(2)
fractional coordinates	x	y	z	
Sc(1)	0.135(5)	0.5	0.486(2)	
Sc(2)	0.191(2)	0.5	0.136(5)	
Sc(3)	0.468(2)	0.5	0.184(5)	
O(4)	0.326(1)	0.5	0.035(4)	
O(5)	0.291(3)	0.5	0.377(4)	
O(6)	0.126(6)	0.0	0.279(7)	
O(7)	0.468(3)	0.0	0.342(5)	
O(8)	0.0	0.5	0.0	

with symmetry C_{3i}, C_2, and C_1, respectively. At ambient conditions, all diffraction peaks can be indexed to a pure cubic-type structure ($Ia\bar{3}$) Sc_2O_3 crystal with space group No. 206 and lattice constants $a = b = c = 9.905(3)$ Å by the Rietveld refinement method (Figure 3a), in agreement with previous reports.[36,37] The number of molecules per unit cell (Z) for this phase is 16, and the volume per molecule $V_0 = 60.74(1)$ Å^3.

A number of typical one-dimensional XRD patterns were collected by increasing the pressure gradually up to 46.2 GPa, as shown in Figure 2. With increasing pressure, the diffraction lines shift toward higher 2θ angles accompanied by a change of the relative intensities. The cubic structure of Sc_2O_3 is stable up to 36 GPa with some of the Bragg peaks merged into broad diffraction peaks and the intensities of some peaks diminished. At pressures higher than 36 GPa, new diffraction peaks start to appear in the XRD patterns (Figure 2), indicating the onset of a structural phase transition. The new diffraction peaks become gradually stronger with an increase of the pressure and become quite distinctive when it reaches 43.4 GPa at the completion of the phase transition. There is a large pressure range where the two phases coexist, which might be explained as being due to the large kinetic effects of the first-order transition. It was reported previously

that phase transition takes place from C to A at 40.9 GPa by shock recovery experiments.[26] Our Rietveld refinement for this new high-pressure phase using a B-type structural model (space group $C2/m$) at 43.4 GPa yields a very good fit with $Rwp = 4\%$ (Figure 3b), suggesting the phase transition sequence is C → B for Sc_2O_3 by static high pressure. Up to 46.2 GPa, the highest pressure in this study, we did not find the phase transition of Sc_2O_3 from B → A. This is in disagreement with the shock-wave results.[26] The lattice parameters refined within this space group for the new phase were $a = 13.142(2)$ Å, $b = 3.221(4)$ Å, $c = 7.773(4)$ Å, and $\beta = 100.55(2)°$ and the volume per molecule is $V_0 = 53.9$ Å^3 ($Z = 6$). High-pressure B-Sc_2O_3 has a different atomic arrangement, containing three nonequivalent point symmetry C_s coordination Sc^{3+} ions within the lattice of O^{2-} ions and with O atoms located at Wyckoff positions 4i, and 2b, as shown in Figure 1b. The unit-cell parameters and atomic positions of the high-pressure phase are given in Table 1. The experimental values are in good agreement with previous reports using the high-temperature and high-pressure method.[24] In Figure 2, the top panel shows the XRD pattern for the structure of Sc_2O_3 after the pressure is released. It indicates that the phase change from C to B is irreversible and Sc_2O_3 remains in the new phase even after the pressure is released. This phenomenon was also found in Eu_2O_3, Yb_2O_3, and Er_2O_3 by previous researchers,

(36) Knop, O.; Hartley, J. M. *Can. J. Chem.* **1968**, *46*, 1446.
(37) Schleid, T.; Meyer, G. *J. Less-Common Met.* **1989**, *149*, 73.
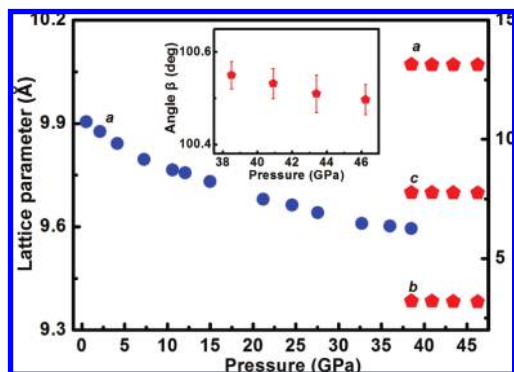
Figure 4. Variation of the lattice parameters of Sc_2O_3 phases as a function of the pressure. The solid blue circles represent C-Sc_2O_3. The solid red pentagons represent B-Sc_2O_3. The inset shows the behavior of the β angle of the B-Sc_2O_3 phase.
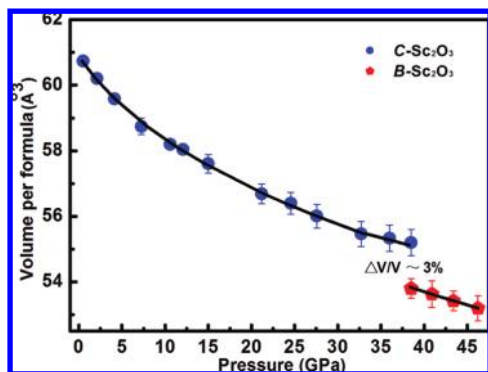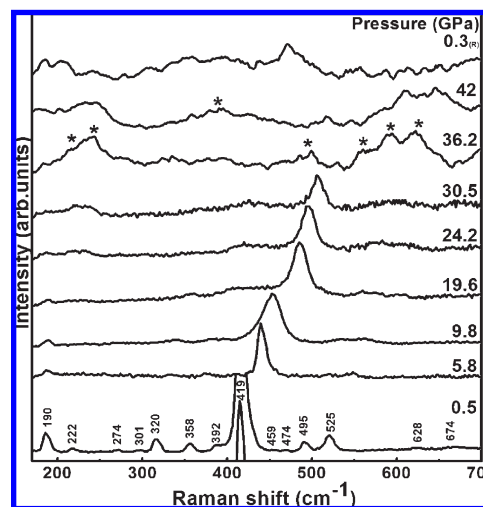

Figure 5. Molar volume as a function of the pressure for Sc_2O_3 phases at pressures up to 46.2 GPa. The solid blue circles represent C-Sc_2O_3 phase data. The solid red pentagons represent B-Sc_2O_3 phase data. The solid black lines are the third-order Birch−Murnaghan equation-of-state fits to $Ia\bar{3}$ and $C2/m$ phase data. Around 36 GPa, there is an estimated volume collapse of 3% from the $Ia\bar{3}$ phase to the $C2/m$ phase.

who attributed it to the high kinetic barrier related to crystal reconstruction.[13,16,38]

Figure 4 shows the normalized cell parameters of two phases over the entire pressure range as functions of pressure, as obtained from refinements of angle-dispersive synchrotron XRD data for Sc_2O_3. The present data display a smooth and monotonic behavior with a pressure up to 36 GPa for the C phase. The changes of lattice parameters a, b, c and the monoclinic angle for the B phase over the pressure range of 36−46.2 GPa are found to be 1.5%, 0.8%, 1.1%, and 0.3%, respectively. In order to determine the bulk modulus B_0, its pressure derivative B_0', and the molar volume at ambient conditions V_0, a third-order Birch−Murnaghan equation-of-state fit of the changes in the relative unit-cell volume with pressure (Figure 5) yields

$$P = 3/2B_0[(V_0/V)^{7/3}$$
$$-(V_0/V)^{5/3}]\{1+3/4(B_0'-4)[(V_0/V)^{2/3}-1]\} \quad (1)$$

where B_0 is the bulk modulus and B_0' is the pressure derivative. We determined the bulk modulus of the C-Sc_2O_3 phase to be $B_0 = 154(5)$ GPa at a fixed $B_0' = 7$. Furthermore, the increase of coordination from C-Sc_2O_3 to B-Sc_2O_3 phases induces a significant volume collapse, about 3%. The result is

(38) Guo, Q. X.; Zhao, Y. S.; Jiang, C.; Mao, W. L.; Wang, Z. W.; Zhang, J. Z.; Wang, Y. J. *Inorg. Chem.* **2007**, *46*, 6164.

Figure 6. Raman spectra recorded the nonreversible structural transition of Sc_2O_3 at different pressures in 100−700 cm^{-1} frequency regions. The assignment of the experimentally observed Raman peaks is based on the theoretical analysis. Asterisks show the appearance of new peaks corresponding to B-Sc_2O_3. The top panel is a Raman spectrum at 0.3 GPa after decompressing from 42 GPa.

slightly lower than the previously reported value of 7.8%.[24] A bulk modulus $B_0 = 180(8)$ GPa at a fixed $B_0' = 4$ for B-Sc_2O_3 was estimated from the data at high pressures. The phase transition is accompanied by breaking of the chemical bonds between atoms and reconstruction of the anion and cation sublattices.

The structural phase transition of Sc_2O_3 was also studied using in situ Raman spectra at high pressures. It provides valuable information on local and cooperative changes during pressure-related transformations between phases. Figure 6 shows some representative Raman spectra of Sc_2O_3 in the frequency range of 100−700 cm^{-1} at different pressures. Because the structure is body-centered, the unit cell contains the primitive structure twice, so that eight unit formulas are used to theoretically determine the number of vibrations. The irreducible representation for the optical and acoustical modes is given as

$$\Gamma = 4A_g + 4E_g + 14F_g + 5A_{2u} + 5E_u + 16F_u \quad (2)$$

where A_g, E_g, and F_g are Raman-active, F_u is IR-active, and A_{2u} and E_u are inactive.[39,40]

The high-pressure B-type-phase structure has a side-centered cell that contains six unit formulas. There are 21 Raman-active modes ($14A_g + 7B_g$) by group analysis at the Brillouin zone ($q = 0$).[41] It should be noted that none of the total of 22 Raman-active modes of cubic Sc_2O_3 shows the predicted number. At ambient conditions, most of the Raman spectra of Sc_2O_3 can be observed to have 14 bands (Figure 6). It is clear that the strongest Raman mode for the cubic Sc_2O_3 is centered at 419 cm^{-1}. The major peak has been assigned as a combination of A_g and F_g modes.[40,42]
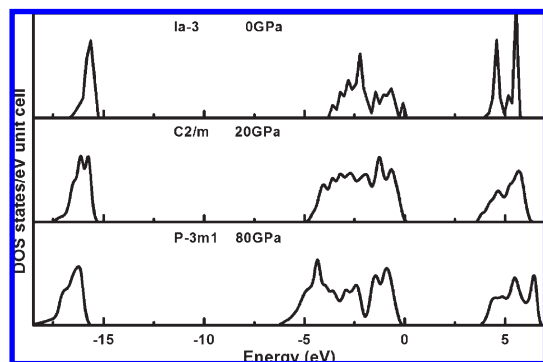
(39) White, W. B.; Keramidas, V. G. *Spectrochim. Acta* **1972**, *28A*, 501.
(40) Repelin, Y.; Proust, C.; Husson, E.; Beny, J. M. *J. Solid State Chem.* **1995**, *118*, 163.
(41) Hongo, T.; Kondo, K.; Nakamura, K. G.; Atou, T. *J. Mater. Sci.* **2007**, *42*, 2582.
(42) Kaminskii, A. A.; Bagaev, S. N.; Ueda, K.; Takaichi, K.; Lu, J.; Shirakawa, A.; Yagi, H.; Yanagitani, T.; Eichler, H. J.; Rhee, H. *Laser Phys. Lett.* **2005**, *2*, 30.

Figure 7. Calculated dispersive curve in the Brillouin zone and the electron DOSs for the $Ia\bar{3}$, $C2/m$, and $P\bar{3}m1$ phases of Sc_2O_3.

Our results are in good agreement with the result of Ubaldini and Carnasciali.[6] The strongest Raman band is expected to be more sensitive to changes in the chemical bonding of Sc_2O_3, which indicates a large polarizability change during the vibration. It is clear from Figure 6 that, up to a pressure of 30.5 GPa, all modes display continuous shifts to higher wavenumbers, indicating a contraction of Sc−O bonds under high pressures. For the Raman spectrum at 36.2 GPa, all Raman vibrational modes of the C-Sc_2O_3 phase vanish entirely. The Raman spectrum consists of a broad background with very weak peaks at around 215, 239, 388, 498, 560, 591, and 621 cm^{-1}. As per the assignments available and taking into account the shifts due to the increase in pressure, these new Raman peaks may be assigned to the B-type phase of Sc_2O_3. These Raman features at high pressures suggest that a structural phase transition has begun at 36.2 GPa in Sc_2O_3 from C-Sc_2O_3 to B-Sc_2O_3 at room temperature, which is in good agreement with the XRD data. As can be seen in Figure 6, upon a total release of pressure, the peaks are still broad but shifted to lower wavenumbers, indicating that the pressure-induced changes are irreversible.

A complementary insight into the high-pressure behavior of Sc_2O_3 can be obtained by carrying out ab initio calculations. The electron density of state (DOS) of Sc_2O_3 at atmospheric pressure was calculated with quantum-mechanical theory, and the results are shown in Figure 7. It is obvious that all three phases C, B, and A of Sc_2O_3 are nonconductive at 0, 20, and 80 GPa, respectively. The polymorphs have similar DOSs, and the band gaps are 3.885, 3.729, and 3.715 eV for the cubic, monoclinic, and hexagonal phases, respectively. The band gaps of different forms are expected to have different optoelectronic properties. Our computational approach is based on constant-pressure static quantum-mechanical calculations at $T = 0$ K, so the relative stability of different phases of Sc_2O_3 can be deduced from the pressure dependence of the enthalpy instead of the Gibbs free energy.[43] Enthalpy difference curves for the cubic, monoclinic, and hexagonal structures of Sc_2O_3 are presented in Figure 8. The calculated enthalpy difference (Figure 8) indicates that the monoclinc B phase becomes thermodynamically more stable than the cubic C phase at 15 GPa. The calculated transition pressure for C → B is significantly lower than what we found experimentally. This discrepancy may be attributed to differences in barrier heights between simulation and experiment.[44]
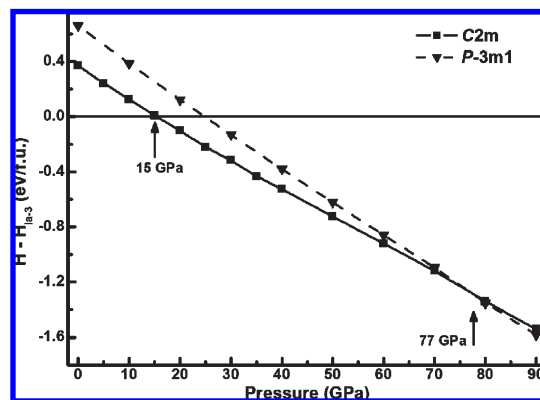
Figure 8. Calculated enthalpies for the $C2/m$ and $P\bar{3}m1$ phases of Sc_2O_3 relative to that of the $Ia\bar{3}$ phase as a function of the pressure. Phase transformations occur at 15 GPa ($Ia\bar{3}$ to $C2/m$) and 77 GPa ($C2/m$ to $P\bar{3}m1$).

The higher barrier heights should induce the higher phase transition point for a system. In our experiment, the Sc_2O_3 crystalline has a barrier, but the calculations do not include a kinetic barrier. Also, it should be noted that our calculations are at zero temperature whereas the experiments were carried out at room temperature.[45] We speculate that all of the above factors may have caused the differences between the experiment and calculation. However, the calculated phase stabilities of the two polymorphs are in agreement with the experimental observations. As seen from Figure 5, the lattice parameters and unit-cell volumes abruptly change at the phase transitions, implying a first-order nature for the phase transitions. The hexagonal A phase becomes energetically more favorable above 77 GPa, indicating the existence of a second phase transition from B-Sc_2O_3 to A-Sc_2O_3, and the transition pressure for B → A agrees well with the theoretical results by Wu et al.[27] Unfortunately, we are not able to extend the pressure up to that range to corroborate the theoretical predictions. The theoretically predicted second high-pressure phase is shown in Figure 1c. We can see that all Sc^{3+} at the 2d sites have point symmetry C_{3v}, which resides in the interstices within the lattice of O^{2-} ions, with two types of O atoms occupying 2d and 1a Wyckoff positions. Our calculated results suggest that the process of the high-pressure phase transition of Sc_2O_3 is from the C to B to A type, consistent with the high-pressure sequence changes of rare-earth sesquioxides at ambient temperature.

5. Conclusions

In summary, we have experimentally confirmed a static high-pressure-induced structural phase transition of Sc_2O_3 using in situ synchrotron-radiation XRD and Raman spectra measurements up to 46.2 and 42 GPa, respectively. The pressure-induced phase transition from the cubic phase to a high-pressure monoclinic phase occurred at 36 GPa, consistent with a previously reported phase transition sequence by a high-temperature and high-pressure method. The structural transitions suggested by variations in the Raman parameters also support our XRD measurements. The pressure−volume data of the new phase of Sc_2O_3 was analyzed using the Birch−Murnaghan equation of state. The zero-pressure bulk

(43) Catti, M. *Phys. Rev. B* **2005**, *72*, 064105.
(44) Chen, C. C.; Herhold, A. B.; Johnson, C. S.; Alivisatos, A. P. *Science* **1997**, *276*, 398.

(45) Karazhanov, S. Zh.; Ravindran, P.; Vajeeston, P.; Ulyashin, A.; Finstad, T. G.; Fjellvåg, H. *Rev. B* **2007**, *76*, 075129.

modulus is $B_0 = 180(8)$ GPa, and its pressure derivative is $B_0' = 4$ for B-Sc_2O_3. Our complementary DFT calculations based on GGA confirm the experimental results and show a pressure-induced phase transition from the C-Sc_2O_3 to B-Sc_2O_3 structure. The calculations also suggest the occurrence of a second pressure-induced phase transition from the B-Sc_2O_3 to A-Sc_2O_3 structure. These results should be helpful in evaluating their production under different synthesis conditions and understanding the physical properties of Sc_2O_3.

Supporting Information Available: $P-T$ schematic diagram of Sc_2O_3 at high pressure and high temperature and observed and calculated d-spacing values of the $C2/m$ structure of Sc_2O_3 at 43.4 GPa. This material is available free of charge via the Internet at http://pubs.acs.org.